Graphical Models 74 (2012) 221–232

Contents lists available at SciVerse ScienceDirect

Graphical Models

journal homepage: www.elsevier.com/locate/gmod

Continuous and discrete Mexican hat wavelet transforms on manifolds

Tingbo Hou *, Hong Qin

Department of Computer Science, Stony Brook University, United States

ARTICLE INFO

Article history:
Available online 7 May 2012

Keywords:
Mexican hat wavelet
Heat diffusion
Biharmonic wavelet
Feature detection
Geometry processing

ABSTRACT

This paper systematically studies the well-known Mexican hat wavelet (MHW) on manifold geometry, including its derivation, properties, transforms, and applications. The MHW is rigorously derived from the heat kernel by taking the negative first-order derivative with respect to time. As a solution to the heat equation, it has a clear initial condition: the Laplace–Beltrami operator. Following a popular methodology in mathematics, we analyze the MHW and its transforms from a Fourier perspective. By formulating Fourier transforms of bivariate kernels and convolutions, we obtain its explicit expression in the Fourier domain, which is a scaled differential operator continuously dilated via heat diffusion. The MHW is localized in both space and frequency, which enables space-frequency analysis of input functions. We defined its continuous and discrete transforms as convolutions of bivariate kernels, and propose a fast method to compute convolutions by Fourier transform. To broaden its application scope, we apply the MHW to graphics problems of feature detection and geometry processing.

1. Introduction

One long-lasting task in geometry processing is to develop functional analysis tools on curved surfaces. Without Euclidean metric, it is extremely challenging to explicitly define functions on manifolds. Many existing methods are hinged upon differential geometry, where surface parameterization is frequently unavoidable. In this work, we study and develop functional analysis tools in frequency domain via spectral decomposition. Functions that have no closed-form expression on manifolds may have explicit formulations in frequency domain. The fundamental goal of this paper is to articulate this spectral approach with mathematical rigor, by studying the Mexican hat wavelet (MHW) and its transforms on manifolds.

Wavelet transforms are important tools for functional analysis and processing. One way to construct discrete wavelets on surfaces is via subdivision. As a regular domain with refining schemes, subdivision is convenient for subsampling and filter banks, which iteratively refine mesh geometry and functions. Subdivision wavelets heavily rely on subdivision connectivity of the mesh, which limits the application scope to data compression and level-of-detail rendering. The regularly-refined hierarchy is, however, computationally expensive and perhaps hard to build. Consequently, it gives rise to a strong demand in flexibly adapted wavelet tools without building the subdivision explicitly, which can be used for fast space-frequency analysis. For data compression, orthogonality is a crucial property of wavelets, while for space-frequency analysis, localization in both space and frequency is much more desirable. This requires wavelets are localized in space and frequency. It also implies the significance of analyzing functions in frequency domain.

In this paper, we advocate the well-known MHW on manifold geometry that is rigorously derived from heat diffusion. Analogous to the Euclidean MHW, the manifold MHW is defined as the negative first-order derivative of the heat kernel with respect to time. As a solution to the heat diffusion partial differential equation (PDE), it takes

* Corresponding author. Address: Room 2426, Computer Science Building, Stony Brook University, Stony Brook, NY 11794-4400, United States.

E-mail addresses: thou@cs.stonybrook.edu (T. Hou), qin@cs.stonybrook.edu (H. Qin).

1524-0703/$ - see front matter © 2012 Elsevier Inc. All rights reserved.
http://dx.doi.org/10.1016/j.gmod.2012.04.010

the Laplace–Beltrami operator as the initial condition. By defining Fourier transforms of bivariate kernels and convolutions, we further reveal that in the Fourier domain, the MHW is a product of the Laplace–Beltrami operator and the heat kernel. It is, therefore, a scaled differential operator continuously dilated through heat diffusion. It has Gaussian decays in both space and frequency, which implies it can extract information in a space-frequency window. We discuss some important properties of the MHW, such as admissibility, convergence, informativeness, and stableness. Moreover, we define its continuous and discrete transforms as convolutions of bivariate kernels. Similar with the case in signal processing, we propose a method to compute convolutions by Fourier transform, which significantly improves the computational time of wavelet transforms, without reducing their accuracy. Applications in feature detection and spectral geometry processing will immediately follow suit after we reveal the MHW's theoretic insights and document its most important properties. As an analog on manifold geometry, it is poised to excite more applications. While the central theme of this paper is studying the MHW and its transforms on manifolds, other contributions can be summarized as follows:

- We study Fourier transforms of bivariate kernels and convolutions on manifolds, with the purpose for function design in the Fourier domain.
- We approach the MHW transforms via Fourier decomposition. We show this Fourier method significantly reduces the complexity while preserving the accuracy.
- Based on the MHW theory, we formulate inverse transforms of continuous and discrete MHWs, which are concise and fast to compute.
- We devise immediate applications of the MHW in space-frequency analysis, including feature detection and spectral geometry processing.
- The proposed mechanism can be extended to other self-adjoint (differential) operators for functional analysis on manifolds.

2. Related work

This section briefly reviews previous work of Fourier transforms and wavelets adapted to manifold geometry.

2.1. Adapted Fourier transforms

Local areas of curved surfaces are homogeneous to 2D planar patches, where the Euclidean Fourier transform can be applied for spectral processing [20]. In terms of adapting the Fourier transform on manifolds, basis functions are critical for orthogonally decomposing the space to a series of shape spectra. In [2,13], eigenfunctions of the symmetric Laplacian of the connectivity graph are adopted as a Fourier basis, which is derived from the mesh topology but not the geometry. Analogous to the Fourier basis in Euclidean metric, manifolds have similar orthonormal basis formed by eigenfunctions of the Laplace–Beltrami operator [15]. Accordingly, Vallet and Lévy [27] defined the manifold harmonic transform (MHT) that is a fully adapted manifold Fourier transform, expanded on manifold harmonics (i.e., Laplace–Beltrami eigenfunctions). For applications, Rong et al. [22] employed this spectral decomposition to perform mesh editing on the base domain with low frequencies and reconstruct details with high frequencies. The Fourier basis, consisting of functions repeatedly oscillating over the entire domain, does not have localization in space. Therefore, adapted Fourier transforms only allow global operations of input functions.

2.2. Adapted wavelets

Defining wavelets on manifolds is never an easy task. One construction on meshed surfaces is achieved via explicit subdivision, which relies on the subdivision connectivity of the mesh. In [24], the lifting scheme is introduced for constructing subdivision wavelets on sphere. Lounsbery et al. [16] studied multiresolution analysis of wavelets constructed on surfaces of arbitrary topological type. In [3], B-spline wavelets are combined with the lifting scheme for biorthogonal wavelet construction. To avoid remeshing, Valette and Prost [26] extended the subdivision wavelet for triangular meshes using irregular subdivision scheme that can be directly computed on irregular meshes. On spherical domains, Haar wavelets [19] are constructed over nested triangular grids generated by subdivision. Recently, the spherical Haar wavelet basis was improved to the SOHO wavelet basis [14] that is both orthogonal and symmetric. In subdivision wavelets, the dilation of scaling functions strictly follows the subdivision scheme, which depends on the meshing. The subdivision wavelets have been frequently used for geometry compression and level-of-detail data visualization. It requires constructing the subdivision hierarchy before defining wavelets, which may limit its application scope. The regularly-refined hierarchy is computationally expensive and perhaps even harder to build.

Other than subdivision, a bottom-up construction of discrete diffusion wavelets [7] has been proposed on graphs and manifolds. They use a diffusion operator and its powers to build the nested subspaces, where scaling functions and wavelets are obtained by orthogonalization and rank-revealing compression. However, the constructed scaling and wavelet functions are not localized. In [18], the biorthogonal diffusion wavelets are introduced, relieving the excessively-strict orthogonality property of scaling functions. Rustamov [23] studied the relation between mesh editing and diffusion wavelets by introducing the generalized linear editing. The diffusion wavelets, iteratively constructed by matrix powers, are inconvenient for low-frequency processing.

In recent research results, mathematicians studied generating wavelets through the use of spectral theory. Hammond et al. [10] addressed graph wavelets through spectral graph theory. The graph wavelets are generated by a wavelet operator expanded on eigenfunctions of the graph Laplacian. In [1], Antoine et al. also studied continuous wavelet transforms on graphs, constructed by a generator in spectral domain. As an example, they introduced the Mexican hat wavelet formulated by the generator $u^2e^{-u^2}$ that is the Fourier transform of the Euclidean MHW. A similar result on compact manifolds was given

in [8]. In this paper, instead of adopting the generator, we derive the MHW from the negative first derivative of the heat kernel with respect to time. Since the heat kernel, as a fundamental solution to the heat equation, has an expansion with separated components of space and time, this derivation is easy to perform. Moreover, it has meaningful relations with the heat kernel and is relevant to the Laplace–Beltrami operator from the perspective of physics-based partial differential equations.

3. Bivariate kernel and convolution on manifolds

In this section, we introduce Fourier transforms of bivariate kernels and convolutions on manifolds, which are necessary in defining our wavelets. In Euclidean domain, the Fourier transform of an integrable function $f(x)$ is defined as

$$\hat{f}(\omega) = \int_{-\infty}^{\infty} f(x) e^{-i\omega x} dx, \tag{1}$$

where $e^{-i\omega x}$ is the Fourier basis, and ω is the frequency. By Euler's formula, the Fourier basis ends up with sine and cosine functions, which are orthonormal and oscillating over the domain. They can be interpreted as eigenfunctions of derivative operators with respect to x. For example, $e^{-i\omega x}$ is the eigenfunction of the second-order derivative operator associated with the eigenvalue ω^2, because of

$$\frac{d^2}{dx^2} e^{-i\omega x} = \omega^2 e^{-i\omega x}. \tag{2}$$

That is, by taking the Fourier basis as eigenfunctions of the second-order derivative operator, the eigenvalues are real numbers corresponding to the squares of frequencies.

For a compact manifold M, the Laplace–Beltrami operator Δ_M is negative and formally self-adjoint, which has a well-defined eigen-system $\{\lambda_k, \phi_k\}$:

$$\Delta_M \phi_k(x) = -\lambda_k \phi_k(x), \tag{3}$$

where λ_k and $\phi_k(x)$ are the kth eigenvalue and the kth eigenfunction, respectively. Analogous to the Fourier basis in Euclidean domain, eigenfunctions $\{\phi_k\}$ form an orthogonal and complete basis for the Hilbert space $L^2(M)$. Therefore, a function $f(x) \in L^2(M)$ can be expanded on this basis,

$$f(x) = \sum_{k=0}^{\infty} \hat{f}(k) \phi_k(x), \text{ where } \hat{f}(k) = \langle f(x), \phi_k(x) \rangle. \tag{4}$$

With a slight abuse of language, we call $\hat{f}(k)$ the Fourier transform, or Fourier coefficient, of function $f(x)$ on manifold M. In [27], it is also called as the manifold harmonics transform (MHT).

With the purpose for space-frequency analysis and filter design for novel wavelet formulation, we consider a bivariate kernel $\theta(x, y)$ of a self-adjoint operator Θ, and explicitly employ such kernel to compute the convolution

$$\theta(x,y) * f(x) = \Theta f(x) = \langle \theta(x,y), f(y) \rangle. \tag{5}$$

The bivariate kernel can be expanded on the Fourier basis

$$\theta(x,y) = \sum_{k=0}^{\infty} \hat{\theta}(k) \phi_k(x) \phi_k(y), \tag{6}$$

where $\hat{\theta}(k)$ is the Fourier transform defined as

$$\hat{\theta}(k) = \langle \langle \theta(x,y), \phi_k(x) \rangle, \phi_k(y) \rangle. \tag{7}$$

Note that off-diagonal entries in frequency are ignored, because of the orthogonality of the Fourier basis.

Table 1 documents some important examples of functions and kernels under the Fourier transform. A Dirac function and a basis function are dualities under the Fourier transform. The impulse function in space has infinite bands in frequency, and vice versa.

We extend the Fourier transform to the convolution by the following theorem.

Theorem 1 (Convolution Theorem). *The Fourier transform of a convolution $\theta(x, y) * f(x)$ is the point-wise product of Fourier transforms $\hat{\theta}(k)\hat{f}(k)$.*

Proof. By definition, we have the Fourier transform of the convolution

$$\begin{aligned} \langle \langle \theta(x,y), f(y) \rangle, \phi_k(x) \rangle &= \langle \langle \theta(x,y), \phi_k(x) \rangle, f(y) \rangle \\ &= \langle \hat{\theta}(k) \phi_k(y), f(y) \rangle = \hat{\theta}(k) \hat{f}(k). \end{aligned}$$

Hence, the statement is proved. □

This theorem facilitates designing functions on manifolds in Fourier domain by concatenation. Functions with complex forms on manifolds may have simple expression in the Fourier domain. One can design new functions by concatenations of known functions in the Fourier domain. For example, our Mexican hat wavelet is formulated as the product of the Laplace–Beltrami kernel and the heat kernel in the Fourier domain: $\hat{\psi}_t(k) = \lambda_k e^{-\lambda_k t}$.

As introduced in [10], the graph Fourier transform satisfies the Parseval's relation. It is easy to see that this relation also holds on manifolds. We give the theorem and proof of this relation below for completeness.

Theorem 2 (Parseval's Theorem [10]). *For any functions $f(x), g(x) \in L^2(M)$, the following relation holds*

$$\langle f(x), g(x) \rangle = \sum_{k=0}^{\infty} \hat{f}(k) \hat{g}(k). \tag{8}$$

Proof. By definition, we have

$$\begin{aligned} \sum_{k=0}^{\infty} \hat{f}(k) \hat{g}(k) &= \sum_{k=0}^{\infty} \langle f(x), \phi_k(x) \rangle \hat{g}(k) = \langle f(x), \sum_{k=0}^{\infty} \hat{g}(k) \phi_k(x) \rangle \\ &= \langle f(x), g(x) \rangle. \end{aligned}$$

Table 1
Some manifold functions and kernels under the Fourier transform.

Function/Kernel	Space	Fourier
Dirac function	$\delta_x(y)$	$\phi_k(x)$
Fourier basis function	$\phi_j(x)$	$\delta_j(k)$
Convolution	$\theta(x, y) * f(x)$	$\hat{\theta}(k)\hat{f}(k)$
Laplace–Beltrami kernel	$\Delta_M(x, y)$	λ_k
Heat kernel	$h_t(x, y)$	$e^{-\lambda_k t}$
Mexican hat wavelet	$\psi_t(x, y)$	$\lambda_k e^{-\lambda_k t}$
Biharmonic wavelet kernel	$\psi_t^2(x, y)$	$\lambda_k^2 e^{-\lambda_k t}$

Hence, the statement is proved. □

This theorem implies the energy conservation in space and frequency. It is an important property of the manifold Fourier transform, which will be used for the perturbation analysis of quantities defined in spectral domain.

4. Mexican hat wavelet and its Fourier transform on manifolds

4.1. Derivation

We derive the MHW on manifolds directly from the heat equation:

$$\frac{\partial u(x,t)}{\partial t} - \Delta_M u(x,t) = 0. \tag{9}$$

The fundamental solution to this PDE is known to be the heat kernel $h_t(x,y) : \mathbb{R}^+ \times M \times M \to \mathbb{R}^+$, given by formulations in space and Fourier domain

$$\begin{cases} h_t(x,y) = \sum_{k=0}^{\infty} e^{-\lambda_k t} \phi_k(x) \phi_k(y) \\ \hat{h}_t(k) = e^{-\lambda_k t}. \end{cases} \tag{10}$$

The heat kernel in Fourier domain $\hat{h}_t(k)$ is a Gaussian of $\sqrt{\lambda_k}$. This implies that, although the heat kernel has no closed-form expression in space, it has an explicit expression as a Gaussian in the Fourier domain.

Recall that the Euclidean MHW is defined as the negative first-order derivative with respect to t (or, equivalently second-order derivative with respect to x) of the Gaussian. We define the MHW $\psi_t(x,y) : \mathbb{R}^+ \times M \times M \to \mathbb{R}$ on manifold geometry as the negative first-order derivative of the heat kernel:

$$\begin{cases} \psi_t(x,y) = \sum_{k=0}^{\infty} \lambda_k e^{-\lambda_k t} \phi_k(x) \phi_k(y) \\ \hat{\psi}_t(k) = \lambda_k e^{-\lambda_k t} = \widehat{\Delta}_M(k) \hat{h}_t(k). \end{cases} \tag{11}$$

This is a solution to the heat equation with the Laplace–Beltrami operator as the initial condition. By the Convolution Theorem 1, the MHW in Fourier domain is the product of the Laplace–Beltrami kernel and the heat kernel, as shown in Table 1. This means that it is a scaled differential operator dilated by heat diffusion.

Here, t is related to "frequency". Different from the frequency index k in Fourier transform, the index t is continuous, leading to a continuous wavelet. Small values of t correspond to high frequencies, while large values correspond to low frequencies, which is opposite to Fourier index k. In the same spirit of diffusion wavelets [7], the MHW uses diffusion for dilation and scaling. Diffusion wavelets smooth the space by discrete powers of a diffusion operator, while the MHW performs this task by continuous heat diffusion subject to the heat equation.

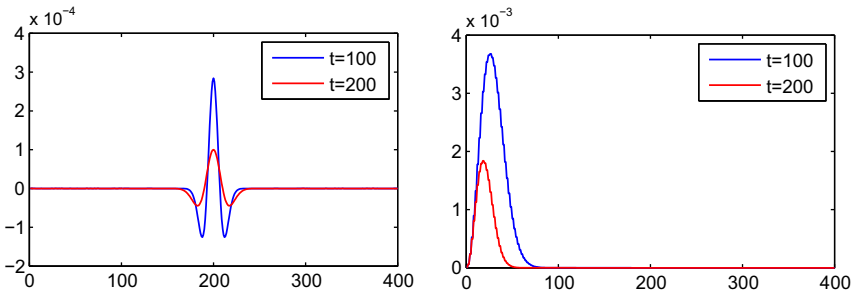

Fig. 1. *Left*: two MHW functions on a 1D manifold with 400 uniformly sampled points. *Right*: their Fourier transforms in frequency domain. For a larger scale (red curves), the MHW has a wider window in space, but a narrower window in frequency.

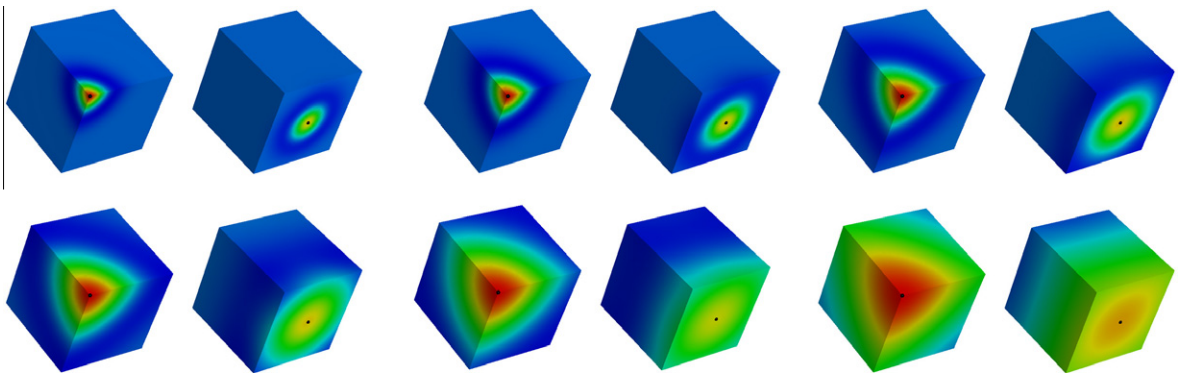

Fig. 2. Mexican hat wavelets on a box at $t = 10, 20, 40, 80, 160, 320$. The centers of functions are marked by black balls. The MHW behaves differently at a corner point and a planar point.

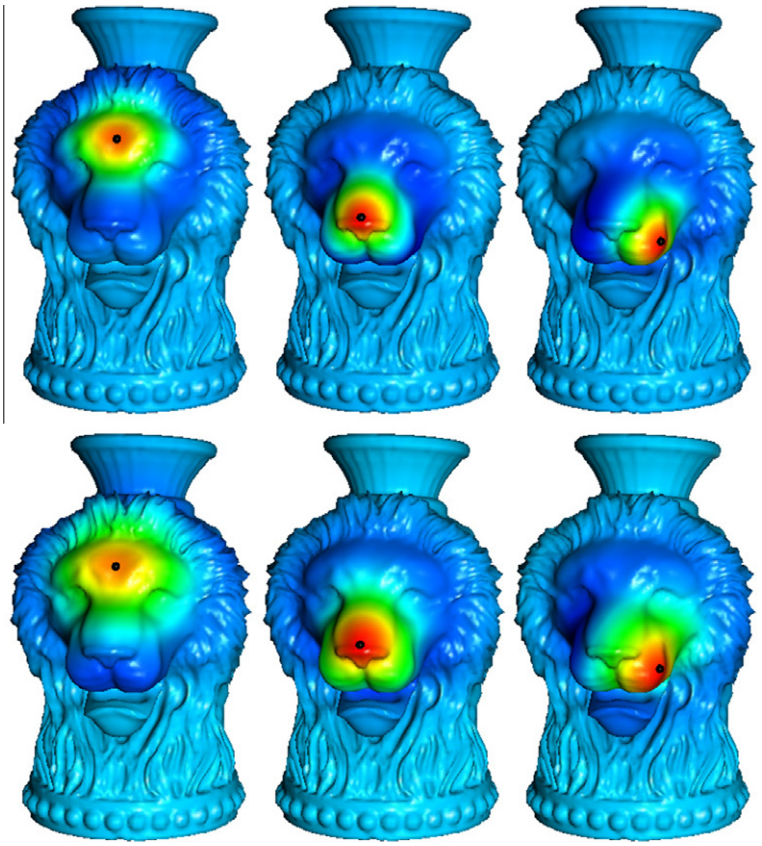

Fig. 3. Some Mexican hat wavelets on a 2D manifold visualized by color plots, at $t = 50$ (*Top*) and $t = 100$ (*Bottom*). Wavelets are attenuated and oscillating on the manifold.

Driven by different applications, the diffusion wavelets do not have oscillating and attenuated shapes.

Fig. 1 shows two MHWs on a 1D manifold with 400 uniformly sampled points, and their Fourier transforms in frequency domain. The MHW has Gaussian decays in both space and frequency. The figure illustrates that for a larger scale (red curves), the MHW has a wider window in space, but a narrower window in frequency. This indicates both space and frequency resolutions cannot be arbitrarily high. The sampling of the MHW in space and frequency follows the Heisenberg principle [12]. Fig. 2 shows some Mexican hat wavelets on a box. The MHW behaves differently at a corner point and a planar point. In Fig. 3, we show some wavelets on a 2D manifold by color-coding. The center points are shown as dark balls. The red-to-blue color illustrates the shown wavelets have similar shapes of the 1D wavelets, which are oscillating and attenuated on the manifold. Fig. 4 visualizes $\psi_t(x, x)$ at different values of t on deformable shapes. The MHW is relevant to shape geometry, and invariant to isometric deformation.

This above scheme for defining wavelets can be extended to other self-adjoint operators. For instance, we define the pth MHW as,

$$\psi_t^p(x,y) = \sum_{k=0}^{\infty} \lambda_k^p e^{-\lambda_k t} \phi_k(x) \phi_k(y). \tag{12}$$

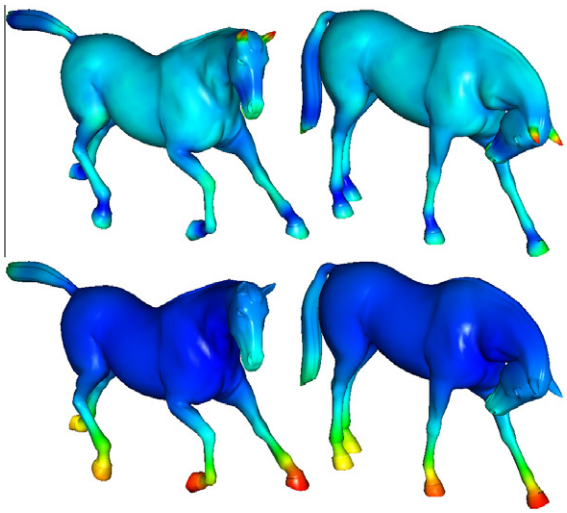

Fig. 4. Visualizing $\psi_t(x, x)$ at $t = 80$ (*Top*) and $t = 640$ (*Bottom*) on deformable shapes. It is relevant to shape geometry, and invariant to isometric deformation.

The order $p > 0$ has a damping effect to the exponential attenuation of the wavelets in Fourier domain. Specifically,

for $p = 2$, it is the biharmonic wavelet, with respect to the biharmonic operator $(\Delta)^2$, as shown in Table 1.

4.2. Properties

We further elaborate some important properties of the MHW on manifolds.

4.2.1. Symmetry

The MHW is symmetric in space, i.e.,

$$\psi_t(x,y) = \psi_t(y,x). \tag{13}$$

4.2.2. Zero-mean

The MHW has a zero mean, given by

$$\int_M \psi_t(x,y)d\mu(y) = 0, \text{ for all } t > 0, \tag{14}$$

where $\mu(y)$ denotes the Riemannian volume of y on the manifold. This is a direct consequence of a property of the heat kernel on stochastically complete manifolds [11],

$$\int_M h_t(x,y)d\mu(y) = 1, \text{ for all } t > 0. \tag{15}$$

It implies that the wavelet $\psi_t(x, y)$ vanishes at zero-frequency in its Fourier transform. In fact, as $\lambda_0 = 0$ for the Neumann Laplace–Beltrami operator [5], the Fourier transform has $\hat{\psi}_t(0) = 0$.

4.2.3. Gaussian-decay

The MHW has Gaussian decays in both space and frequency. In frequency, the Fourier transform $\hat{\psi}_t(k) = \lambda_k e^{-\lambda_k t}$ has a Gaussian decay. In space, the heat kernel and its derivatives have a Gaussian upper bound [4], which implies a Gaussian decay on the manifold with given t. Hence, the MHW drops exponentially to zero along the manifold. This is also related to the multiscale property of the heat kernel, which states that for small value of t, the heat kernel $h_t(x, \cdot)$ is mostly determined by a small neighborhood of x. The Gaussian decay indicates that, although not locally-supported, the MHW is localized in space and frequency [21].

4.2.4. Admissibility

The admissibility condition of wavelets is to ensure the function can be inversely recovered after transforms. We first formally define the admissibility condition for wavelets on manifolds as follows:

Definition 1 (*Admissibility Condition*). On compact Riemannian manifolds, a wavelet ψ is *admissible*, or equivalently satisfies the *admissibility condition*, if and only if

$$\sum_{k=0}^{\infty} \frac{|\hat{\psi}(k)|^2}{k} < \infty.$$

Theorem 3 (Admissibility Theorem). *The manifold Mexican Hat Wavelet is admissible.*

Proof. We have the Fourier transform of the MHW: $\hat{\psi}_t(k) = \lambda_k e^{-\lambda_k t}$. By recalling the Weyl's Theorem [5], eigenvalues have an asymptotic formula. It yields that, for a 2-manifold M, the eigenvalue λ_k can be approximated by ck, with some positive constant c determined by $\mu(M)$. Therefore, we have

$$\frac{|\hat{\psi}(k)|^2}{k} = \frac{\lambda_k^2 e^{-2\lambda_k t}}{k} < c_1 k e^{-c_2 k t},$$

with positive constants c_1 and c_2, and

$$\sum_{k=0}^{\infty} \frac{|\hat{\psi}(k)|^2}{k} < \sum_{k=0}^{\infty} c_1 k e^{-c_2 k t} < \frac{c_1}{c_2 t} < \infty.$$

Hence, the WHW is admissible. □

4.2.5. Convergence

The long-time $\psi_t(x, y)$ converges to a stable state,

$$\lim_{t\to\infty} \psi_t(x,y) = 0, \text{ for all } x, y \in M. \tag{16}$$

It means for large value of t, $\psi_t(x, y)$ converges to zero everywhere on the manifold, which is the state of zero-frequency. It is based on the fact that, for a manifold with bounded geometry $\mu(M) < \infty$, we have a stable state of the heat kernel [9]

$$\lim_{t\to\infty} h_t(x,y) = \frac{1}{\mu(M)}, \text{ for all } x, y \in M. \tag{17}$$

which is constant everywhere on M.

The short-time $\psi_t(x, y)$ converges to the Laplace–Beltrami kernel

$$\lim_{t\to 0^+} \psi_t(x,y) = \sum_{k=0}^{\infty} \lambda_k \phi_k(x)\phi_k(y) = \Delta_M(x,y). \tag{18}$$

This convergence once again demonstrates the deep bond between the MHW and the Laplace–Beltrami operator.

4.2.6. Informativeness

Similar to the heat kernel, the wavelet $\psi_t(x, y)$ is also informative. This property is abstracted as the following statement.

Theorem 4 (Informative Theorem). *Let $T: M \to N$ be a bijective map between manifolds M and N. If $\psi_t^M(x,y) = \psi_t^N(T(x), T(y))$ for all $x, y \in M$ and all $t > 0$, then we have $h_t^M(x,y) = h_t^N(T(x), T(y))$, and T is isometric.*

Proof. By definition, we have

$$\int_0^t \psi_t(x,y)dt = h_0(x,y) - h_t(x,y).$$

By the Dirac condition [9], we have $h_0(x,y) = \delta(x,y)$. Considering that T is a bijective map, if $\psi_t^M(x,y) = \psi_t^N(T(x), T(y))$ for all $x, y \in M$ and all $t > 0$, then we have $h_t^M(x,y) = h_t^N(T(x), T(y))$. And by the Proposition 2 in [25], T is isometric. □

This theorem implies that the isometric geometry can be completely determined by the MHW. Hence, it is informative. It captures the geometry up to isometry.

4.2.7. Stableness

The construction of wavelets ψ_t from their Fourier transforms $\hat{\psi}_t$ in spectral domain is stable. That is, perturbations of wavelets in frequency will not be amplified after inverse Fourier transform.

Theorem 5 (Perturbation Theorem [10]). *For two Fourier transforms $\hat{\psi}_t(k), \hat{\psi}'_t(k)$, if $\sum_{k=0}^{\infty}\left(\hat{\psi}_t(k)-\hat{\psi}'_t(k)\right)^2 \leqslant \epsilon(t)$, then for any $x \in M$, $\|\psi_t(x,y)-\psi'_t(x,y)\|^2 \leqslant \epsilon(t)$.*

Proof. By the Parseval's Theorem 2, we have

$$\left\|\psi_t-\psi'_t\right\|^2 = \langle(\psi_t-\psi'_t),(\psi_t-\psi'_t)\rangle = \sum_{k=0}^{\infty}\left(\hat{\psi}_t(k)-\hat{\psi}'_t(k)\right)^2 \leqslant \epsilon(t). \quad \square$$

This property means the computation of MHW is stable under perturbations of its Fourier coefficients, and hence the Laplace–Beltrami eigenvalues.

5. MHW transforms: a Fourier perspective

In this section, we analyze continuous wavelet transform (CWT) and discrete wavelet transform (DWT) of the MHW from a Fourier perspective.

Theorem 6 (CWT of the MHW). *For any function $f(x) \in L^2(M)$, the CWT and its Fourier transform are given by*

$$\begin{cases} \mathcal{W}_f^{\psi}(x,t) = \psi_t(x,y) * f(x) \\ \widehat{\mathcal{W}}_f^{\psi}(k) = \hat{\psi}_t(k)\hat{f}(k) \end{cases}. \tag{19}$$

The inverse CWT is given by

$$f(x) = \int_0^{\infty} W_f^{\psi}(x,t)dt + R_f, \tag{20}$$

where $R_f = \hat{f}(0)\phi_0(x)$ is a residual constant.

Proof. Eq. (19) is a direct consequence of the Convolution Theorem 1. For Eq. (20), we have

$$\begin{aligned}\int_0^{\infty}\mathcal{W}_f^{\psi}(x,t)dt &= \int_0^{\infty}\sum_{k=0}^{\infty}\lambda_k e^{-\lambda_k t}\hat{f}(k)\phi_k(x)dt = \sum_{k=1}^{\infty}\hat{f}(k)\phi_k(x) \\ &= f(x)-\hat{f}(0)\phi_0(x).\end{aligned}$$

Hence, the statement is proved. $\square$

In the CWT, x and t are localized in space and frequency, respectively, and $\mathcal{W}_f^{\psi}(x,t)$ is also called the wavelet coefficient of $f(x)$. It records detail information of $f(x)$ at different scales. The convolution-based expression is analogous to the Fourier transform. Its time complexity is quadratic to the data size, since point-to-point function values are required. However, through its Fourier transform, we obtain a spectral expression of the CWT

$$\mathcal{W}_f^{\psi}(x,t) = \sum_{k=0}^{\infty}\lambda_k e^{-\lambda_k t}\hat{f}(k)\phi_k(x), \tag{21}$$

which is only linear to the data size. This is consistent with the case in signal processing, that convolutions can be fast computed by the Fourier transform.

Similarly, we can define the DWT, which will be useful in some applications. Assume we have a discrete sequence of samples $[t_0, t_1, \ldots, t_J]$. For the ease of formulation, we always let $t_0 = 0$, and $[t_1, t_2, \ldots, t_J]$ form a geometric sequence. We define the discrete MHW as

$$\begin{cases} \psi_{t_j}(x,y) = h_{t_{j-1}}(x,y) - h_{t_j}(x,y) \\ \hat{\psi}_{t_j}(k) = \hat{h}_{t_{j-1}}(k) - \hat{h}_{t_j}(k), \end{cases} \tag{22}$$

for $j = 1, 2, \ldots, J$.

Theorem 7 (DWT of the MHW). *For any function $f(x) \in L^2(M)$, the DWT and its Fourier transform are given by*

$$\begin{cases} \mathcal{W}_f^{\psi}(x,t_j) = \psi_{t_j}(x,y) * f(x) \\ \widehat{\mathcal{W}}_f^{\psi}(k) = \hat{\psi}_{t_j}(k)\hat{f}(k), \end{cases} \tag{23}$$

The inverse DWT is given by

$$f(x) = \sum_{j=1}^{J} W_f^{\psi}(x,t_j) + R_f(x,t_J), \tag{24}$$

where $R_f(x,t_J) = h_{t_j}(x,y) * f(x)$ is the residual function.

Proof. Eq. (23) is a direct consequence of the Convolution Theorem 1. For Eq. (24), we have

$$\begin{aligned}\sum_{j=1}^{J} W_f^{\psi}(x,t_j) &= h_{t_0}(x,y) * f(x) - h_{t_j}(x,y) * f(x) \\ &= f(x) - h_{t_j}(x,y) * f(x).\end{aligned}$$

Hence, the statement is proved. $\square$

We also obtain a spectral expression for the DWT:

$$\mathcal{W}_f^{\psi}(x,t_j) = \sum_{k=0}^{\infty}(e^{-\lambda_k t_{j-1}} - e^{-\lambda_k t_j})\hat{f}(k)\phi_k(x). \tag{25}$$

The aforementioned (continuous and discrete) inverse transforms imply that we can, without loss of any information, recover a signal from its wavelet coefficients and a residual function. Therefore, they can be used in function approximation and analysis.

6. Applications and experiments

6.1. Implementation and evaluation

For meshed surfaces, we approximate wavelets and their transforms by a relatively small number of eigenfunctions. The eigen-system has a scale problem derived from the Laplace–Beltrami operator. We adopt the scaling method in [28], which uses the mean vertex area as a unit. It makes the selection of t *meaningful*, such that $t = 1$ results in an average influence region of about 1-ring. In Fig. 5, we show accuracy curves of $\psi_t(x,x)$ on a 400-point 1D manifold, computed with different percentages of eigenfunctions. A high accuracy can be achieved by increasing the number of used eigenfunctions. High frequencies (with small t) require more eigenfunctions to maintain the accuracy. This is because in Fourier transform, high frequencies correspond to large values of k. The determination of the number of eigen-

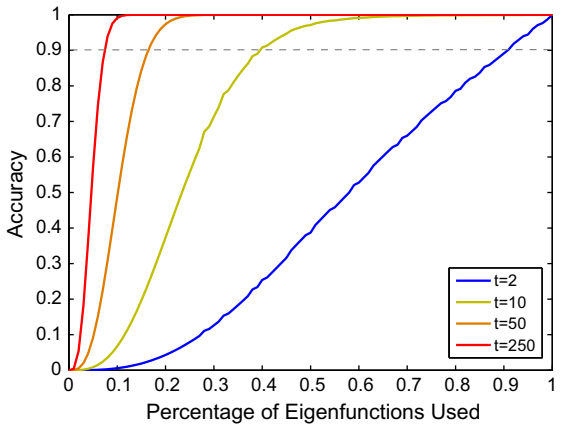

Fig. 5. Accuracy of $\psi_t(x, x)$ on a 400-point 1D manifold, computed with different percentages of eigenfunctions. A high accuracy can be achieved by increasing the number of eigenfunctions used. High frequencies (small t) require more eigenfunctions to maintain accuracy. The determination of the number of eigenfunctions depends on t and the data size.

functions depends on t and the data size. This experiment implies a way to choose proper t in applications.

Assume the number of vertices is V, and the number of used eigenfunctions is K. The time complexity to compute all wavelets $\psi_t(x, y)$ at a t is then $O(KV^2)$, and so is the convolution-based CWT in Eq. (19). This is, however, extremely inconvenient for practical use, since V is usually at the order of tens, maybe even hundreds of thousands. Similar to the case in signal processing, the proposed Fourier method with a spectral expression significantly improves the computation. It has $O(KV)$ time complexity, with the same accuracy of the convolution. Fig. 6 shows the time performance of a wavelet transform computed by convolution (*Left*) and Fourier transform (*Right*), with 10% eigenfunctions used. The horizontal axis denotes data size. The performance of the spectral expression is approximately linear to the data size, which significantly improves the time performance. The spectral expression also enables an efficient method to compute the heat transform and solve the heat equation. Table 2 documents time performance for computing eigen-decomposition (Eigen) and wavelet transform (WT) on selected data in our experiments. Here, we use $K = 300$ for all experiments.

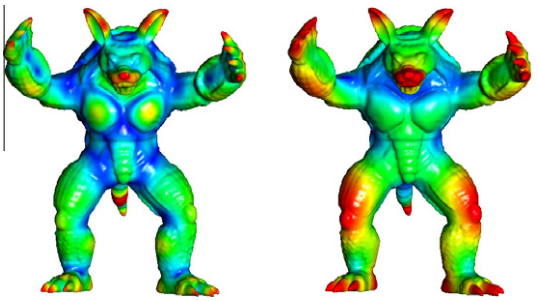

Fig. 7. CWT of vertex coordinates at $t = 10$ (*Left*) and $t = 400$ (*Right*), whose half normal is convergent to the mean curvature as $t \to 0^+$.

6.2. Feature detection

One important application of the MHW is feature detection, since it is sensitive to second derivatives of inputs. For a given function $f(x) \in L^2(M)$, features are recognized as local extrema of its wavelet coefficients $W_f^{\psi}(x, t)$, which are zero-crossings of second-order derivatives. On 2D images, this method is known as the scale invariant feature transform (SIFT) [17].

Specifically, when inputs are vertex coordinates $v = [v_x, v_y, v_z]$ of a meshed surface, the half normal of wavelet coefficients in three dimensions of $\mathbb{R}^3$ is convergent to the mean curvature as $t \to 0^+$. This is because the short-time MHW converges to the Laplace–Beltrami operator, and half normal of $\Delta_M v$ is the mean curvature. Fig. 7 shows CWT maps of vertex coordinates at $t = 10$ and $t = 400$ on the Armadillo. Fig. 8 gives some results of feature detection, where features are shown as green balls whose sizes depend on their scales.

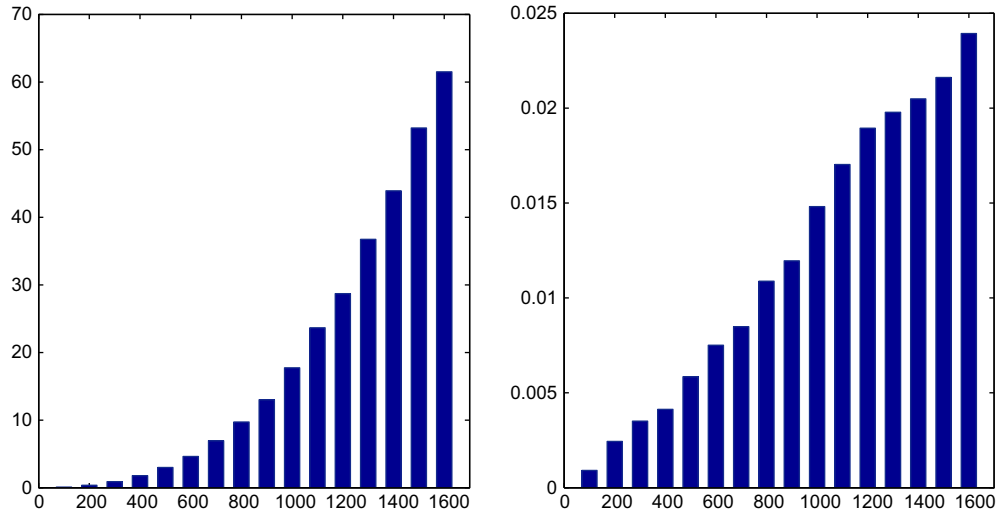

Fig. 6. Time performance of computing wavelet transform by convolution (*Left*) and Fourier transform (*Right*), with 10% eigenfunctions used. The horizontal axis denotes data size. The Fourier method significantly improves the time performance.

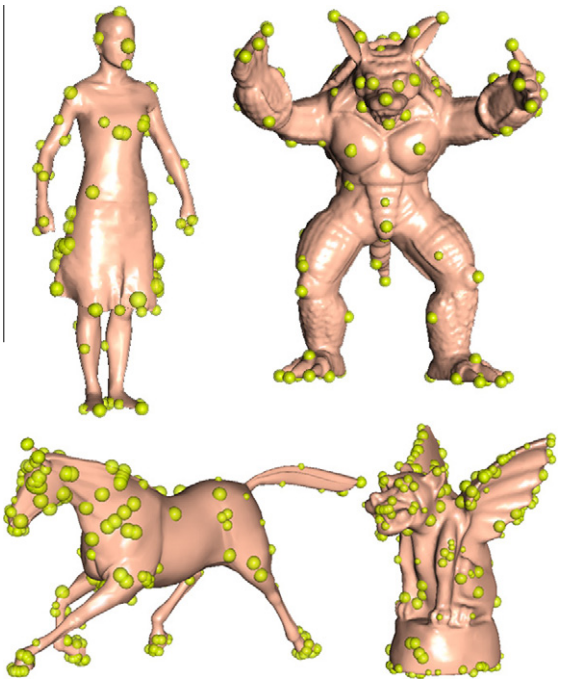

Fig. 8. Examples of feature detection.

In these examples, only features with wavelet coefficients larger than a threshold $\sigma = \text{mean}(\|W_v^{\psi}\|)$ are shown.

6.3. Spectral geometry processing

Spectral geometry processing is referred to mesh filtering in frequency domain [27]. The filtering of mesh geometry can also be achieved by solving a Poisson equation [6]. In this application, we use the DWT. An input shape is decomposed to wavelet coefficients at different scales, and a residual shape $R_t(x, t_J)$. Fig. 9 shows residual shapes and magnitudes of wavelet transforms. Details are gradually "peeled off" from the residual shape, and ready for analysis. With the spectral expression, we can rapidly compute spectral decomposition at any scale. Wavelet coefficients extract geometry information at different scales. A common spectral processing is to apply filters to coefficients at different frequencies. The output shape is obtained by inverse DWT of filtered wavelet coefficients and a residual shape.

Consider results shown in [27], shapes are usually processed with low-pass, enhancement, and band exaggeration filters, resulting in global effects of smoothing, enhancing, and mixture, respectively. The same effects can be achieved by the MHW, with some results shown in Fig. 10. Only for the MHW, we do not need to compute full eigen-system of the Laplace–Beltrami operator, since

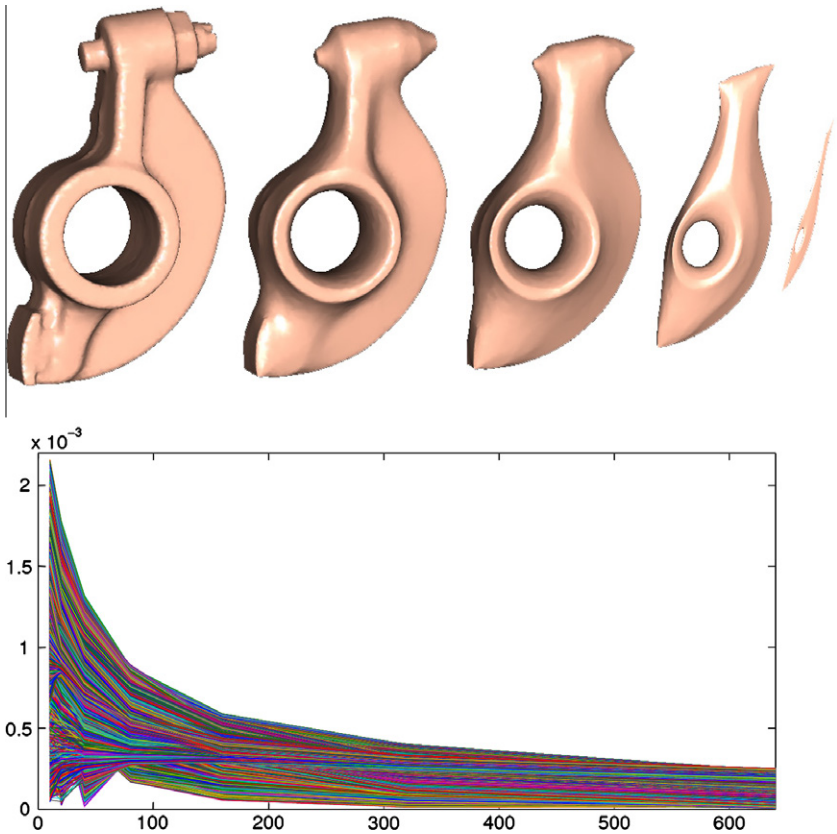

Fig. 9. *Top*: residual shapes $R_t(x,t_j)$ at different scales with $t_J = 0, 10, 40, 160, 640$. *Bottom*: magnitudes of wavelet transforms $|W_v^{\psi}(x,t)|$ along t.

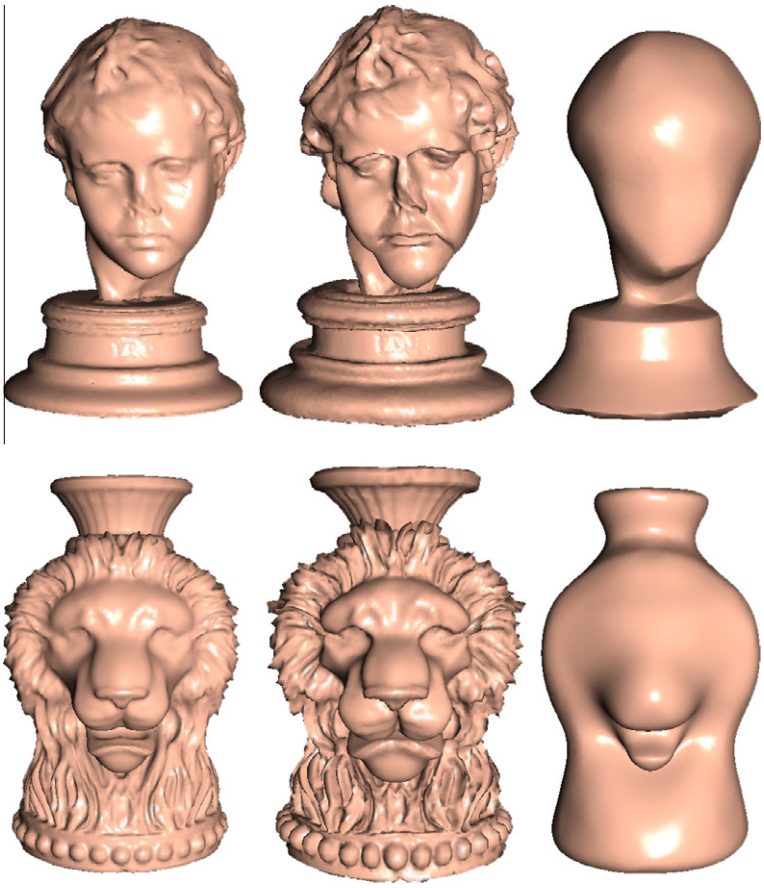

Fig. 10. Global filtering of input shapes, from *Left* to *Right*: original shapes, enhanced shapes, and smoothed shapes.

a small number of eigenfunctions are accurate enough for selected scales. As shown in Table 2, our computation is very fast. Moreover, the decomposition by DWT is lossless, with all high-frequency information stored in $W_v^{\psi}(x,t_1)$.

Moreover, the processing can be spatially different by the MHW, since it has localization in both space and frequency. It can perform space-frequency analysis on geometry. Accordingly, we can apply space-frequency filters in geometry processing, given by

$$v(x)=\sum_{j=1}^{J}\Gamma(x,t_j)W_v^{\psi}(x,t_j)+R_f(x,t_J), \tag{26}$$

where $\Gamma(x,t_j)$ is a filter localized in place x and frequency t_j. This allows local operations of spectral processing on geometry. In this paper, we design some space-frequency filters along with some lower-frequency Laplace–Beltrami eigenfunctions and show some results, in Fig. 11. Precisely, a linear filter along $\phi_k(x)$

$$\Gamma(x,t_j)=\frac{1.5(\phi_k(x)-\min(\phi_k(x)))}{\max(\phi_k(x))-\min(\phi_k(x))}+0.5, \tag{27}$$

is applied to all $W_v^{\psi}(x,t_j)$. Using these filters, the input shape is gradually morphed from smoothing to enhancement. Other types of filters can also be designed according to specific applications.

Table 2
Time performance (in s) for computing eigen-decomposition (Eigen) and wavelet transform (WT).

Data	V	Level	Eigen	WT
Armadillo (Fig. 7)	50,000	5	139.93	1.09
Woman (Fig. 8)	9971	3	28.36	0.11
Rocker (Fig. 9)	10,044	5	30.16	0.12
Eros (Fig. 10)	25,651	3	69.62	0.26
Lion (Fig. 11)	23,889	4	64.38	0.29
Fish (Fig. 11)	24,975	4	67.59	0.34

7. Discussion and conclusion

In this paper, we have detailed the MHW and its transforms on manifold geometry. It is solely derived from the heat equation. By means of formulating bivariate kernels for differential operators and their Fourier transforms, we obtain an explicit spectral expression of the MHW. This strongly advocates a novel approach to developing functional analysis tools in Fourier domain. The MHW has localization in both space and frequency, hence having a strong appeal to applications in space-frequency analysis. The proposed Fourier method for computing convolutions of wavelet transforms is stable and efficient, which is con-

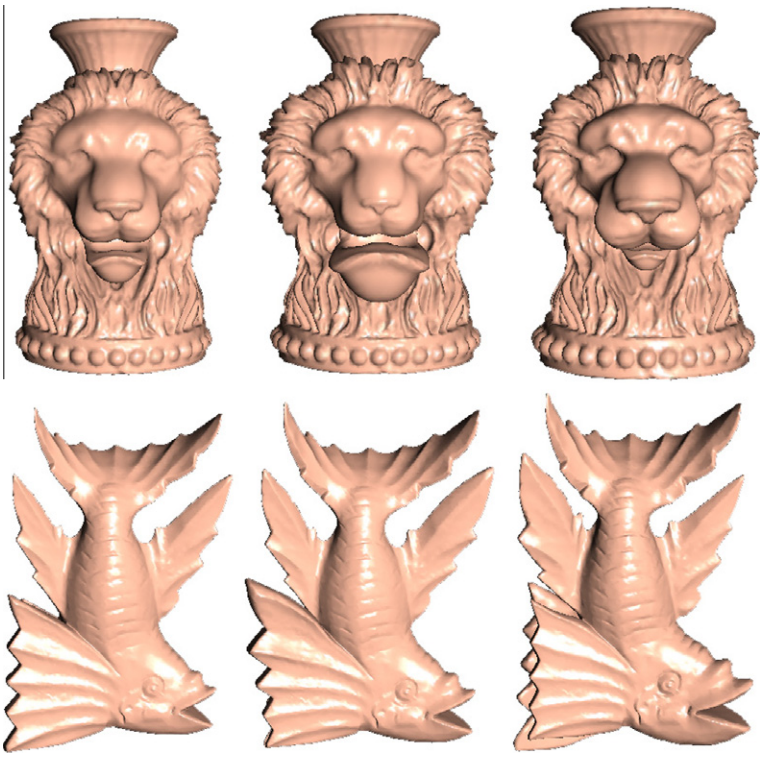

Fig. 11. Space-frequency filtering of input shapes. From *Left* to *Right*: original shapes, and two columns of filtered shapes. The filters are linear to some lower-frequency Laplace–Beltrami eigenfunctions.

sistent with the case in signal processing. Closely related to the Laplace–Beltrami operator, the MHW captures important information in geometry. Therefore, it has the potential to serve as a good descriptor for shape representation and comparison.

Several other issues that require further comprehensive studies, include boundary conditions, eigen-problems for other types of initial-value partial differential equations and their corresponding operators, and more and broader applications. For partial shapes with boundaries, imposing stochastic completeness leads to inconsistent values of the MHW near boundaries. And the affected area becomes larger when t increases. Fast solving the eigen-problem of the Laplace–Beltrami operator is another challenge. Particularly, for the Fourier transform and derived spectral expressions, they require the eigenfunctions to be strictly orthonormal. For applications, we plan to broaden their scope in space-frequency analysis of deformable shapes.

Acknowledgments

This research is supported in part by d US National Science Foundation Grants IIS-1047715, IIS-1049448, IIS-0949467, and IIS-0710819. Models are courtesy of the AIM@SHAPE repository.

References

[1] J.-P. Antoine, D. Roşca, P. Vandergheynst, Wavelet transform on manifolds: old and new approaches, Applied and Computational Harmonic Analysis 28 (2) (2010) 189–202.
[2] M. Ben-Chen, C. Gotsman, On the optimality of spectral compression of mesh data, ACM Transactions on Graphics 24 (1) (2005) 60–80.
[3] M. Bertram, M.A. Duchaineau, B. Hamann, K.I. Joy, Generalized b-spline subdivision-surface wavelets for geometry compression, IEEE Transactions on Visualization and Computer Graphics 10 (3) (2004) 326–338.
[4] A. Boggess, A. Raich, Heat kernels, smoothness estimates and exponential decay. ArXiv e-prints, 2010.
[5] I. Chavel, Eigenvalues in Riemannian Geometry, Academic Press, 1984.
[6] M. Chuang, M. Kazhdan, Interactive and anisotropic geometry processing using the screened poisson equation, ACM Transactions on Graphics 30 (4) (2011) 57:1–57:10.
[7] R.R. Coifman, M. Maggioni, Diffusion wavelets, Applied and Computational Harmonic Analysis 21 (1) (2006) 53–94.
[8] D. Geller, A. Mayeli, Continuous wavelets on compact manifolds, Mathematische Zeitschrift 262 (4) (2008) 895–927.
[9] A. Grigor'yan, Heat kernels on weighted manifolds and applications, Contemporary Mathematics 398 (2006) 93–191.
[10] D.K. Hammond, P. Vandergheynst, R. Gribonval, Wavelets on graphs via spectral graph theory, Applied Computational Harmonic Analysis 30 (2) (2011) 129–150.
[11] P. Hsu, Heat semigroup on a complete Riemannian manifold, The Annals of Probability 17 (3) (1989) 1248–1254.
[12] S. Jaffard, Y. Meyer, R.D. Ryan, Wavelets: Tools for Science & Technology, SIAM, 2001.
[13] Z. Karni, C. Gotsman, Spectral compression of mesh geometry, in: ACM SIGGRAPH, 2000, pp. 279–286.
[14] C. Lessig, E. Fiume, Soho: orthogonal and symmetric haar wavelets on the sphere, ACM Transactions on Graphics 27 (1) (2008) 4:1–4:11.
[15] B. Lévy, Laplace–Beltrami eigenfunctions towards an algorithm that "understands" geometry, in: Shape Modeling International, 2006, pp. 13–20.
[16] M. Lounsbery, T.D. DeRose, J. Warren, Multiresolution analysis for surfaces of arbitrary topological type, ACM Transactions on Graphics 16 (1) (1997) 34–73.
[17] D. Lowe, Distinctive image features from scale-invariant keypoints, International Journal of Computer Vision 60 (2) (2004) 91–110.
[18] M. Maggioni, J. Bremer, R.R. Coifman, A. Szlam, Biorthogonal diffusion wavelets for multiscale representations on manifolds and graphs, in: SPIE Wavelets XI, vol. 5914, 2005, pp. 1–13.

[19] G.M. Nielson, I.-H. Jung, J. Sung, Haar wavelets over triangular domains with applications to multiresolution models for flow over a sphere, in: IEEE Visualization, 1997, pp. 143–150.
[20] M. Pauly, M. Gross, Spectral processing of point-sampled geometry, in: ACM SIGGRAPH, 2001, pp. 379–386.
[21] D. Roşca, J.-P. Andrei, Locally supported orthogonal wavelet bases on the sphere via stereographic projection, Mathematical Problems in Engineering (2009).
[22] G. Rong, Y. Cao, X. Guo, Spectral mesh deformation, The Visual Computer 24 (7) (2008) 787–796.
[23] R.M. Rustamov, On mesh editing, manifold learning, and diffusion wavelets, in: IMA Mathematics of Surfaces XIII, 2009, pp. 307–321.
[24] P. Schröder, W. Sweldens, Spherical wavelets: efficiently representing functions on the sphere, in: ACM SIGGRAPH, 1995, pp. 161–172.
[25] J. Sun, M. Ovsjanikov, L. Guibas, A concise and provably informative multi-scale signature based on heat diffusion, in: Symposium on Geometry Processing, 2009, pp. 1383–1392.
[26] S. Valette, R. Prost, Wavelet-based multiresolution analysis of irregular surface meshes, IEEE Transactions on Visualization and Computer Graphics 10 (2) (2004) 113–122.
[27] B. Vallet, B. Lévy, Spectral geometry processing with manifold harmonics, Computer Graphics Forum 27 (2) (2008) 251–260.
[28] A. Vaxman, M. Ben-Chen, C. Gotsman, A multi-resolution approach to heat kernels on discrete surfaces, ACM Transactions on Graphics 29 (4) (2010) 121:1–121:10.